Frontiers of Information Technology & Electronic Engineering
www.zju.edu.cn/jzus; engineering.cae.cn; www.springerlink.com
ISSN 2095-9184 (print); ISSN 2095-9230 (online)
E-mail: jzus@zju.edu.cn

An efficient quadrature demodulator for medical ultrasound imaging*

Hao ZHOU, Yin-fei ZHENG‡

(*MOE Key Laboratory for Biomedical Engineering, Zhejiang University, Hangzhou 310027, China*)

E-mail: bmezhou@zju.edu.cn; zyfnjupt@126.com

Received June 10, 2014; Revision accepted Oct. 19, 2014; Crosschecked Mar. 6, 2015

Abstract: Quadrature demodulation is used in medical ultrasound imaging to derive the envelope and instantaneous phase of the received radio-frequency (RF) signal. In quadrature demodulation, RF signal is multiplied with the sine and cosine wave reference signal and then low-pass filtered to produce the base-band complex signal, which has high computational complexity. In this paper, we propose an efficient quadrature demodulation method for B-mode and color flow imaging, in which the RF signal is demodulated by a pair of finite impulse response filters without mixing with the reference signal, to reduce the computational complexity. The proposed method was evaluated with simulation and in vivo experiments. From the simulation results, the proposed quadrature demodulation method produced similar normalized residual sum of squares (NRSS) and velocity profile compared with the conventional quadrature demodulation method. In the in vivo color flow imaging experiments, the time of the demodulation process was 5.66 ms and 3.36 ms, for the conventional method and the proposed method, respectively. These results indicated that the proposed method can maintain the performance of quadrature demodulation while reducing computational complexity.

Key words: B-mode ultrasound imaging, Color flow imaging, Quadrature demodulation, Finite impulse response filter

doi:10.1631/FITEE.1400205 **Document code:** A **CLC number:** TP399; TN98

1 Introduction

In ultrasound imaging, radio-frequency (RF) ultrasound waves are transmitted into the body and echoes are received to provide the images of tissue structure, motions of tissue, and blood flow distribution in vessel, for medical diagnostics and therapy guidance. Compared with other commonly used medical imaging modalities, such as X-ray, X-ray CT, and magnetic resonance imaging (MRI), ultrasound imaging is characterized by non-invasion, non-ionization, low cost, and real-time imaging and thus, ultrasound imaging is playing an important role in clinical use. B-mode, color flow imaging (CFI), and spectral Doppler are still the three major modes of ultrasound imaging for clinical use (Thomas, 2005). In these three modes, demodulation has to be used to obtain the envelope and instantaneous phase of the RF signal before any back-end processing. Generally, there are three types of methods for the demodulation of ultrasound RF signal:

1. Hilbert transform based demodulation: In this method, the analytical signal of the received RF signal is obtained using the Hilbert transform, and the envelope and instantaneous phase can be derived from the module and the phase angle of the analytical signal, respectively (Chang *et al.*, 2007).

2. Filtering of the RF signal based demodulation: Many demodulation methods have been

‡ Corresponding author

* Project supported by the National Key Technology R&D Program of China (No. 2011BAI12B02) and the Fundamental Research Funds for the Central Universities, China (Nos. 2014FZA5019 and 2015FZA5019)

ORCID: Hao ZHOU, http://orcid.org/0000-0001-6894-1139

proposed in which a filter is used to extract the envelope of the RF signal. For example, the rectification of RF signal followed by filter is a simple method for envelope derivation, in which the envelope is derived by low-pass filtering the absolute value of the RF signal (Chang *et al.*, 2007); nonlinear filter can also be applied to the RF signal to detect the envelope of the RF signal (Fritsch *et al.*, 1999). However, filtering based demodulation cannot provide the instantaneous phase of the RF data, and thus this method is not suitable for CFI and spectral Doppler.

3. Quadrature demodulation: In this method, the received RF signal is first multiplied with sine and cosine waveforms, respectively, and the mixed signals are low-pass filtered to generate the complex base-band signal (Chang *et al.*, 2007). As in the Hilbert demodulation, the envelope and the instantaneous phase can be obtained by calculating the module and the phase angle of the derived complex base-band signal.

Generating the analytical signal using the Hilbert transform involves using the fast Fourier transform (FFT) (Marple, 1999; Lee *et al.*, 2012), and would provide the ideal envelope and instantaneous phase angle of the echo signal. However, the Hilbert transform requires a higher computational cost compared with other demodulation methods. The computational complexity of Hilbert transform based demodulation is approximately $O(n \log n)$, whereas the computational complexity of conventional quadrature demodulation is approximately $O(n)$. Therefore, this kind of demodulation method is often limited to off-line processing due to its simple implementation and the ideal complex envelope it provides (Chang *et al.*, 2007). To reduce the computational cost of Hilbert transform based demodulation, approximate Hilbert transform based demodulation was proposed, in which a well designed filter was applied to the band width limited ultrasound signal to produce Hilbert transformed data (Reilly *et al.*, 1994; Levesque and Sawan, 2009; Hassan *et al.*, 2011). However, the real- and imaginary-part of the approximate Hilbert transform demodulation are generated by filters with different characteristics. In CFI and spectral Doppler, the imbalance between the filters would result in biased velocity estimations.

On the other hand, quadrature demodulation is the most commonly used demodulator in commercial ultrasound devices. The low-pass filter in quadrature demodulation limits the band width of the base-band complex signal to suppress the electronic noise, and can improve the image quality and penetration depth of the ultrasound device. Although the efficiency of quadrature demodulation is very high, it still occupies not less than 30% of all the computational resources of the conventional ultrasound imaging system (Pailoor and Pradhan, 2008). Furthermore, to provide more diagnostic information, conventional ultrasound imaging modes are often operated in parallel with newer ultrasound imaging technologies (e.g., coded excitation, elasticity imaging, acoustic radiation force imaging (ARFI), and transient elastography), which requires more computational resource (Palmeri *et al.*, 2006; Zahiri-Azar and Salcudean, 2006; Jin *et al.*, 2010; Zahiri-Azar *et al.*, 2012). As a result, the efficiency of quadrature demodulation needs to be improved further to reduce the high computational burden involved in real-time ultrasound imaging.

The purpose of this paper is to present an efficient quadrature demodulator for medical ultrasound B-mode imaging and CFI. In the proposed method, the received RF signal is demodulated by a pair of FIR filters without mixing with sine and cosine signals. The design of the demodulation FIR filters is presented. The proposed method is evaluated with simulation and in vivo experiments.

2 Methods

2.1 Quadrature demodulation in ultrasound imaging

The sampled and beamformed RF ultrasound signal is referred to as $r(n)$, where n is the sample index ($1 < n < N$, N is the total number of samples of each acquired scan line). Considering the band-pass characteristics of the ultrasound transducer, $r(n)$ can be described as a narrow band signal:

$$r(n) = a(n)\cos(\omega_c n + \varphi(n)), \tag{1}$$

where $a(n)$ is the envelope of the received signal, $\omega_c = 2\pi f_c T_s$ (f_c is the central frequency of the transducer and T_s is the sampling interval), and $\varphi(n)$ is the instantaneous phase of the received signal. Generally, the structure information of the tissue is contained in the envelope of $r(n)$ and the motion information of the moving tissue is contained in the instantaneous phase of $r(n)$.

To obtain the envelope and instantaneous phase of the received signal, quadrature demodulation would be applied to the sampled signal. As shown in Fig. 1a, in quadrature demodulation, the sampled signal is multiplied with sine and cosine signals with a frequency of f_c and low-pass filtered. The in-phase and quadrature components of the quadrature demodulator, $I(n)$ and $Q(n)$, can be denoted as

$$\begin{cases} I(n)=\sum_{i=0}^{M}h(i)\left[r(n-i)\cos(\omega_c(n-i)+\varphi_c)\right], \\ Q(n)=\sum_{i=0}^{M}h(i)\left[r(n-i)\sin(\omega_c(n-i)+\varphi_c)\right], \end{cases} \tag{2}$$

where $h(i)$ is the impulse response of the low-pass filter, φ_c is the initial phase of the sine and cosine signals used in mixing, and M is the order of the digital low-pass filter. Note that both the infinite impulse response (IIR) filter and finite impulse response (FIR) filter can be used for low-pass filtering the mixed signal. Because FIR filters are stable, linearly phased, and can be implemented easily using parallel computing (Gerneth, 2010), FIR filters with an order of M are used in this study. Using Eq. (1) and trigonometric identities and considering the passband of the FIR low-pass filter, the complex base-band signal of quadrature demodulation can be written as

$$\begin{aligned} e(n)&=I(n)+\mathrm{j}Q(n)\\ &=\sum_{i=0}^{M}h(i)\left[\frac{a(n-i)}{2}\cos(\varphi(n-i)-\varphi_c)\right]\\ &\quad-\mathrm{j}\sum_{i=0}^{M}h(i)\left[\frac{a(n-i)}{2}\sin(\varphi(n-i)-\varphi_c)\right]\\ &\approx\frac{a(n-d)}{2}\exp(\mathrm{j}\varphi_c)\exp\left[-\mathrm{j}\varphi(n-d)\right], \end{aligned} \tag{3}$$

where j denotes the imaginary unit and d is the group delay of the FIR low-pass filter (refer to the Appendix for the detailed derivation of Eq. (3)).

1. Quadrature demodulation for B-mode imaging

The envelope of the RF signal $\mathrm{env}(n)$ used in B-mode imaging can be obtained by taking the module of $e(n)$ directly:

$$\mathrm{env}(n)=2|e(n)|=a(n-d). \tag{4}$$

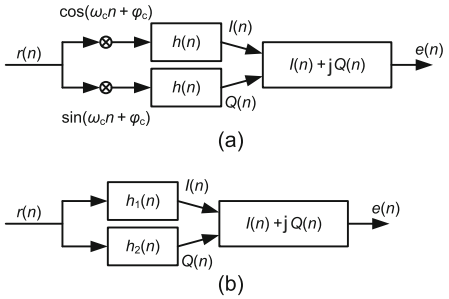

Fig. 1 Block diagrams of conventional quadrature demodulation (a) and the proposed demodulation (b). $h(n)$ is the impulse response of the low-pass filter and $h_1(n)$ and $h_2(n)$ are the impulse responses of the proposed filters

2. Quadrature demodulation for color flow imaging

For CFI, multiple ultrasound pulses are transmitted consecutively in a same direction with a repetitive frequency of f_{prf} to sample the moving targets in the vessel. Let $r_k(n)$ denote the received signal after the kth transmission, where k is the transmission index ($0\le k\le K-1$, K is the total number of transmissions or called the 'ensemble size'). Since f_{prf} is relatively large (usually more than 1 kHz), the envelope of the received signal among different transmissions would remain the same, that is,

$$r_k(n)=a(n)\cos(\omega_c n+\varphi_k(n)). \tag{5}$$

To obtain the velocity of the targets, demodulate the received signal sequences and apply auto-correlation between the consecutive received signals:

$$\begin{aligned} x_{\mathrm{auto},k}&=e_k(n)e_{k-1}^{*}(n)\\ &=\frac{a(n-d)}{2}\exp(\mathrm{j}\varphi_c)\exp\left[-\mathrm{j}\varphi_k(n-d)\right]\\ &\quad\cdot\frac{a(n-d)}{2}\exp(-\mathrm{j}\varphi_c)\exp\left[\mathrm{j}\varphi_{k-1}(n-d)\right]\\ &=\frac{a^2(n-d)}{2}\exp\left[\mathrm{j}(\varphi_k(n-d)-\varphi_{k-1}(n-d))\right]. \end{aligned} \tag{6}$$

The velocity of the moving targets can then be derived by taking the phase angle of the averaged $x_{\mathrm{auto},k}$:

$$v=-\frac{cf_{\mathrm{prf}}}{4\pi f_c}\mathrm{Arg}\left(\frac{\sum_{k=1}^{K-1}x_{\mathrm{auto},k}}{K-1}\right), \tag{7}$$

where c is the sound speed in soft tissue and $\mathrm{Arg}(\cdot)$ gives the principal value of the argument of a complex number.

2.2 Efficient quadrature demodulation without reference signal mixing

As shown in Eqs. (4) and (6), since modulation and auto-correlation are performed, the initial phase of the reference sine and cosine waveforms in quadrature demodulation will not influence the results of envelope detection and velocity estimation. Thus, unlike conventional quadrature demodulation, we propose to replace the initial phase φ_c of the reference waveforms used in Eqs. (2) and (3) with $-\omega_c n$, which will not even influence the envelope or velocity estimation. Eq. (2) can now be rewritten as

$$\begin{cases} I(n)=\sum_{i=0}^{M} h(i)\,[r(n-i)\cos(-\omega_c i)], \\ Q(n)=\sum_{i=0}^{M} h(i)\,[r(n-i)\sin(-\omega_c i)], \end{cases} \tag{8}$$

and the corresponding complex signal of the demodulation is

$$\begin{aligned} e(n) &= I(n)+\mathrm{j}Q(n) \\ &= \sum_{i=0}^{M} h(i)\left[\frac{a(n-i)}{2}\cos(\varphi(n-i)+\omega_c n)\right] \\ &\quad -\mathrm{j}\sum_{i=0}^{M} h(i)\left[\frac{a(n-i)}{2}\sin(\varphi(n-i)+\omega_c n)\right] \\ &\approx \frac{a(n-d)}{2}\exp(-\mathrm{j}\omega_c n)\exp\left[-\mathrm{j}\varphi(n-d)\right]. \end{aligned} \tag{9}$$

Eq. (9) is similar to Eq. (3); the factor $\exp(-\mathrm{j}\omega_c n)$ can be eliminated by the operations of modulation and auto-correlation. Eq. (8) indicates that when performing quadrature demodulation using an FIR low-pass filter, the received signal is actually filtered by a pair of filters with their coefficients produced from the multiplications of the impulse response of the low-pass filter and the reference waveform (i.e., $h(i)\cos(-\omega_c i)$ and $h(i)\sin(-\omega_c i)$). Thus, a pair of FIR filters are derived which can be used for quadrature demodulation without mixing the RF signal with the reference signal (Fig. 1b). Note that the complex signal is almost the same as the baseband signal generated by the conventional quadrature demodulation except for an exponential coefficient, $\exp(-\mathrm{j}\omega_c n)$, which can be compensated by modulation and auto-correlation, and thus decimation can be performed directly as in conventional quadrature demodulation.

Although the proposed filter can be designed by simply multiplying the coefficients with the reference waveforms, the symmetry of the linear phase FIR filters and the reference waveforms can be exploited to produce a pair of symmetric filters to further reduce the number of multiplication operations (Fig. 2). Taking this into consideration, the proposed quadrature demodulation filters can be designed by the following two steps (Fig. 2):

1. Design a linear phase low-pass FIR filter with proper characteristics for quadrature demodulation.

2. Multiply the coefficients of the FIR filter in step 1 with the reference waveform as

$$\begin{cases} h_1(n)=h(n)\cos\left(\omega_c n-\dfrac{M}{2}+\dfrac{\pi}{2}\right), \\ h_2(n)=h(n)\sin\left(\omega_c n-\dfrac{M}{2}+\dfrac{\pi}{2}\right), \end{cases} \tag{10}$$

where $h(n)$ is the linear phase low-pass FIR filter with an order of M designed in step 1, and $n=0,1,\cdots,M$. The filter coefficients are generated using Eq. (10) and loaded prior to real-time imaging.

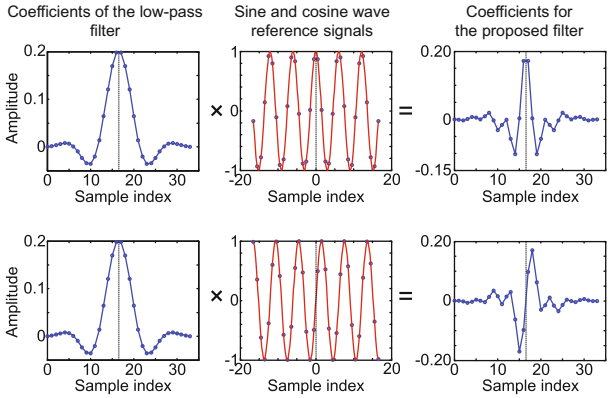

Fig. 2 Diagrammatic explanation of designing the proposed demodulation filters ($M=32$). Top rule: derivation of the filter $h_1(n)$ (even symmetric, for the in-phase component); bottom rule: derivation of the filter $h_2(n)$ (odd symmetric, for the quadrature component)

Suppose the number of samples of a scan line is N and the decimation rate is L after demodulation, the total number of multiplication operations of conventional quadrature demodulation is $2N+2NM/(2L)$, whereas the total number of multiplication operations of the proposed method is $2NM/(2L)$. For example, the sampling frequency

of the ultrasound machine is usually 40 MHz. When using a transducer of a central frequency of 6.6 MHz, the decimation rate can be set to $L = 4$. If the length of the FIR filter is 16, the total number of multiplication operations of the proposed method is only $2 \times 16 \times N/(2 \times 4) = 4N$, compared with $2N + 2 \times 16 \times N/(2 \times 4) = 6N$ for the conventional method.

2.3 Numerical validation

Two simulations were conducted using the computer simulation program Field II (Jensen and Svendsen, 1992) to evaluate the performance of the proposed quadrature demodulator for envelope detection and velocity estimation, respectively. The synthesized RF signal was demodulated by the proposed method and compared with the results of the conventional quadrature demodulation method and the Hilbert transform method. For the proposed method, the low-pass filter used for developing the pair of demodulation filters was the same as that used in the conventional method. The low-pass FIR filters used in the simulations were designed using the Remez algorithm provided by Matlab (MathWorks, USA) and the cut-off frequency of the low-pass filter was set to the transmit frequency (f_c).

2.3.1 B-mode imaging evaluation

In the first simulation, B-mode images of a phantom composed of 12 point targets were formulated (Fig. 3a). A linear array was used to insonify the targets. The frequency-dependent attenuation coefficient was set to 0.5 dB/(cm · MHz) to shift the central frequency of the backscattered ultrasound signal during propagation. An FIR filter with an order of eight was used to demodulate the RF signal. The RF data from the most central scan line was taken out to investigate the accuracy of the proposed method when the order of the filter changes from 8 to 64 and the number of bits of the filter coefficients was set to 10.

The accuracy of the proposed method was evaluated using the normalized residual sum of squares (NRSS) (Levesque and Sawan, 2009):

$$\mathrm{NRSS} = \frac{\sum_{n=0}^{N-1} |c(n) - \mathrm{env}_{\mathrm{Hil}}(n)|^2}{\sum_{n=0}^{N-1} |\mathrm{env}_{\mathrm{Hil}}(n)|^2}, \tag{11}$$

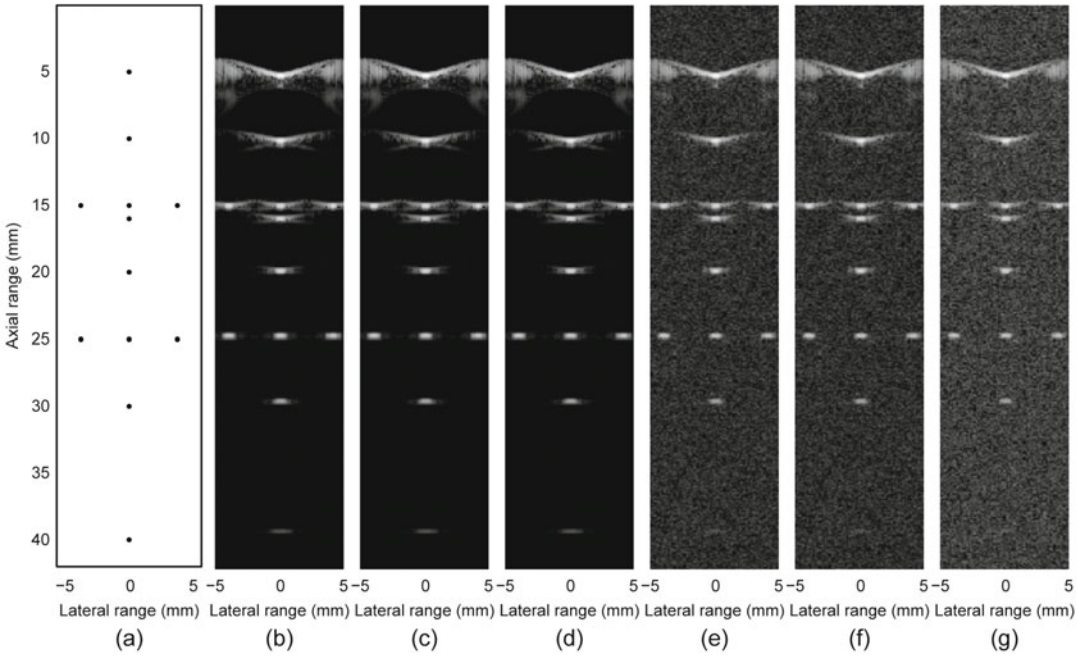

Fig. 3 Simulation results of the B-mode images: (a) 12-target array model; (b) B-mode image without noise and envelope detected by the proposed method; (c) B-mode image without noise and envelope detected by the conventional method; (d) B-mode image without noise and envelope detected by the Hilbert transform method; (e) B-mode image with SNR=20 dB and envelope detected by the proposed method; (f) B-mode image with SNR=20 dB and envelope detected by the conventional method; (g) B-mode image with SNR=20 dB and envelope detected by the Hilbert transform method

where env_{Hil} is the ideal envelope of the RF signal obtained using the Hilbert transform method.

Next, Gaussian white noise was added to the synthesized RF signals to produce a signal-to-noise ratio (SNR) of 20 dB to evaluate the performance in the noise reduction of the proposed method. The parameters used in this simulation are detailed in Table 1.

2.3.2 CFI evaluation

In the second simulation, CFI images of a cylindrical vessel placed at a depth of 2 cm with 30° aligned with respect to the surface of the transducer were synthesized. The scatterers' velocities across the vessel cross section were set to be a parabolic profile with a maximum velocity of 30 cm/s and 0 cm/s on the boundary of the vessel (Zhao *et al.*, 2007). Gaussian white noise was added to the obtained RF signal to give an SNR of 30 dB. An FIR filter with an order of eight was used to demodulate the RF signal to provide the instantaneous phase. The simulation parameters used in this simulation are also listed in Table 1.

2.4 In vivo evaluation

A program for real-time B-mode and CFI was developed based on a Sonix TOUCH ultrasonic imaging system (Ultrasonix, Canada), which is equipped with a 128-element linear transducer array (L14-5/38).

The transmitting and receiving of ultrasound signal was programmed using the Texo software development kit (v6.0.7, Ultrasonix, Analogic Corp., Canada). The transmission sequence was composed of 256 conventional line-by-line B-mode scan lines and 36 beam-interleaved CFI scan lines with a sector size of six and an ensemble size of ten (Zahiri-Azar *et al.*, 2010), which produces a frame rate of 20 for this duplex real-time imaging. As soon as each RF frame has been acquired, quadrature demodulation was performed for each scan line using the proposed method and the conventional method, respectively. Then decimation, envelope detection, logarithm compression, and coordination transform were conducted on the B-mode scan lines. CFI scan lines were processed by wall-filtering, autocorrelation, and velocity estimation. The velocity estimator in Loupas *et al.* (1995) was used to increase the accuracy of velocity estimation. The estimated velocity distribution was color coded and finally superimposed on the B-mode images and displayed on an LCD monitor. The parameters of the ultrasound program are listed in Table 2.

C++ and MFC (Microsoft Visual Studio 2010, Microsoft Corp., USA) were used to implement the real-time imaging software. Since the Sonix TOUCH machine uses a dual-core CPU (Intel E4300 1.8 GHz) and one core of the CPU was totally occupied for acquiring RF signal, a multi-thread technique was used in the program. Since the Sonix TOUCH provides 16-bit fixed point beamformed RF data, the coefficients of the filters used in the demodulation were quantized into a 10-bit fixed point number to improve the efficiency of the program. The streaming SIMD extension (SSE) was also used to maximize the efficiency of the imaging software.

Table 1 Simulation parameters

Parameter	Value	
	B-mode	CFI
Probe type	128-element linear array	128-element linear array
Pitch (mm)	0.3048	0.3048
Kerf (mm)	0.0350	0.0350
Number of active elements	32	32
Transmit frequency (MHz)	6.6	6.6
Fractional bandwidth	80%	80%
Transmit focus distance (mm)	20	20
Sampling frequency (MHz)	40	40
Pulse repeat frequency (Hz)	–	3300

CFI: color flow imaging

Table 2 In vivo experiment parameters

Parameter	Value	
	B-mode	CFI
Probe type	128-element linear array	128-element linear array
Pitch (mm)	0.3048	0.3048
Kerf (mm)	0.0350	0.0350
Number of active elements	32	32
Transmit frequency (MHz)	6.6	5.0
Transmit focus distance (mm)	20	20
Sampling frequency (MHz)	40	20
Number of excitation cycles	1	4
Pulse repeat frequency (Hz)	–	3300
Scan-line space (mm)	0.1524	0.3048
Decimation rate	4	1
Maximum imaging depth (mm)	30	20

CFI: color flow imaging

3 Results

Fig. 3 shows the simulation results of the B-mode images of the 12-target array model. As shown in Figs. 3b–3d, under visual assessments, the performance of the proposed method was similar to those of the conventional quadrature demodulation method and the Hilbert transform based method. As indicated in Figs. 3e and 3f, a similar SNR improvement was obtained by the proposed method and the conventional method when white noise is present. In contrast, the image obtained by the Hilbert transform method suffers from a higher noise level.

Fig. 4 shows the NRSS of the proposed method. The NRSS of the conventional method is also presented. As shown, the accuracy of the envelope detection of the proposed method is similar to that of the conventional method when the same number of taps of the filters was used. Note that a larger number of filter taps will not minimize the NRSS, since the filter with a larger number of taps will produce a higher side-lobe level which worsens the NRSS. The discrepancy of the NRSS between the proposed method and the conventional method results from the use of the fixed number of bits for the coefficients of the filter. If the float-point number for the coefficients of the filters (original filter coefficients generated by Matlab) is used, the proposed method will produce the same NRSS as the conventional quadrature demodulation method.

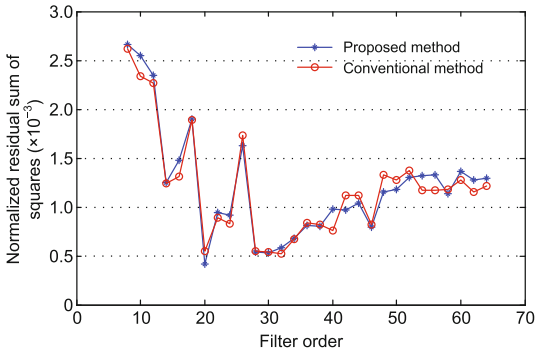

Fig. 4 Normalized residual sum of squares (NRSS) of the proposed method and the conventional quadrature demodulation method (the number of bits of the filter coefficients is 10)

Fig. 5 shows the color flow map obtained by the simulation using the proposed quadrature demodulation method. A flow profile of the simulation is also presented based on 30 random realized simulations and compared with the conventional method and the Hilbert transform method. As shown in Fig. 6, the flow profile obtained by the proposed method matches well with that of the conventional and Hilbert transform methods.

Fig. 7 shows the graphic user interface (GUI) of the developed ultrasound imaging software where the flow velocity map of a healthy common carotid artery (CCA) is presented. The image quality of the color flow map obtained by the proposed method (Fig. 7a) is similar to that of the conventional method (Fig. 7b). In addition, the computing time of the demodulation operation for each frame was 5.66 ms and 3.36 ms for the conventional method and the proposed method, respectively. Since the Loupas velocity estimator was used, decimation was not performed on CFI lines, which makes the improvement of computing time trivial. To investigate the improvement of the frame rate, we turned the CFI mode

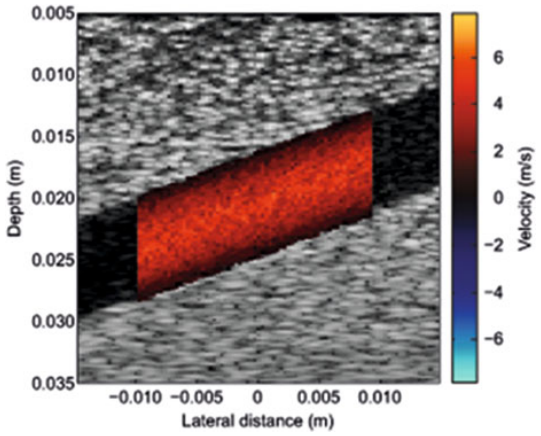

Fig. 5 The color flow map of the vessel model using the proposed quadrature demodulation method. References to color refer to the online version of this figure

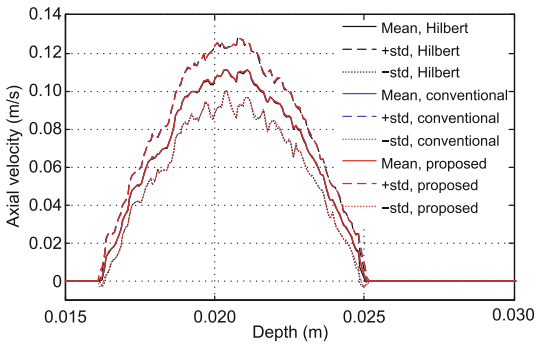

Fig. 6 Detected mean flow velocity and ±1 standard deviation of the center line of the simulation. References to color refer to the online version of this figure

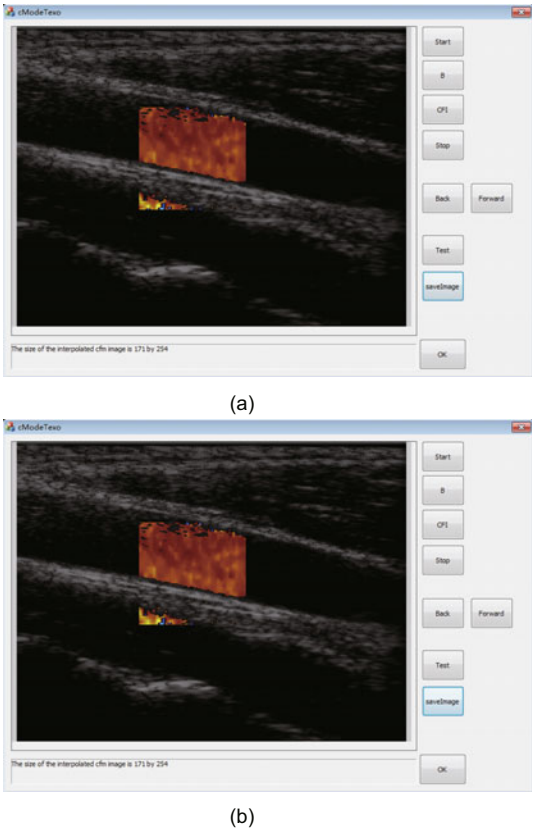

Fig. 7 GUIs using the proposed demodulation method (a) and the conventional quadrature demodulation method (b). The color flow map reveals the velocity distribution in a healthy common carotid artery. References to color refer to the online version of this figure

off and increased the penetration depth of B-mode imaging to 60 mm without changing other parameters in Table 2. At this time, the computing time for generating a B-mode image was 30.77 ms and 27.88 ms for the conventional method and the proposed method, respectively. The corresponding frame rate was 32 frame/s and 35 frame/s, respectively, and a frame rate improvement of 10% was obtained.

4 Discussions

Since the proposed method is developed based on the standard quadrature demodulation method, similar accuracy and SNR improvement have been obtained (Figs. 4, 6, and 7). The proposed method demodulates the RF signal without mixing with the reference signal, and thus speeds up the demodulation process. This efficient demodulation method can be used for improving the frame rate of B-mode imaging, or saving more computational resources without much frame rate loss for incorporating a sophisticated imaging processing method (e.g., speckle reduction and tissue equalization) or advanced imaging modes.

In the conventional quadrature demodulation method, the RF signal (Fig. 8a) is first mixed with the reference (sine and cosine) signal, i.e., a complex exponential signal, so that the spectrum of the RF signal is shifted towards the base-band, and the high-frequency component is dropped out by the low-pass filter to produce the base-band signal (Fig. 8b). In contrast, the filter in the proposed method is designed using Eq. (10), where the coefficients of the low-pass filter are mixed with the reference signal; as a result, the spectrum of the low-pass filter is shifted towards the passband of the RF signal (Fig. 8c) and only the positive (or negative) frequency component of the RF signal is maintained. Thus, the proposed method works like an approximate Hilbert transformer (Fig. 8d). However, compared with the

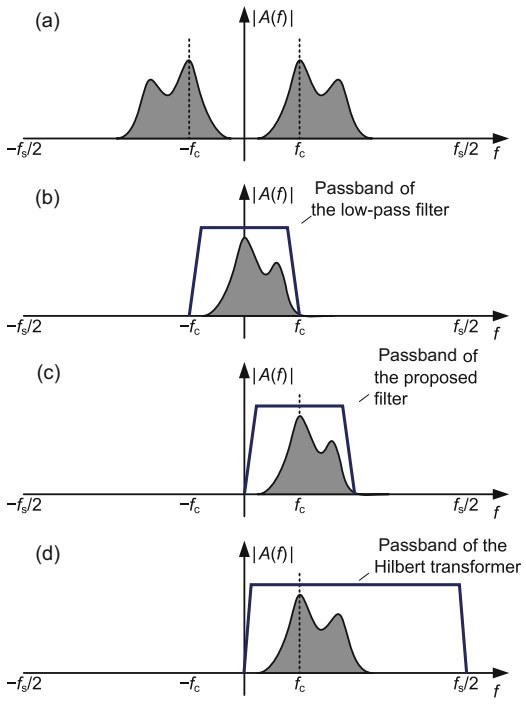

Fig. 8 Comparisons of the proposed method and conventional methods in the frequency domain: (a) spectrum of the radio-frequency (RF) signal; (b) spectrum of the base-band signal after conventional quadrature demodulation; (c) spectrum of the complex signal obtained using the proposed method; (d) spectrum of the complex signal obtained using the approximate Hilbert transform method

conventional approximate Hilbert transformer, the filters in the proposed method are derived from the same low-pass filter and the accuracy of the instantaneous phase is guaranteed. Furthermore, the noise level of the proposed method is lower than that of the Hilbert transform method, since a narrower passband is used.

Although the proposed method is derived based on the beamformed RF signal, it can also be used in phase-rotation-based beamforming (Agarwal *et al.*, 2007). In phase-rotation-based beamforming, the received RF data of each channel is quadrature demodulated, decimated, delayed, phase rotated, and summed. The extra exponential factor contained in the complex signal (Eq. (9)) generated by the proposed method can be eliminated in the 'phase rotated' step, resulting in the same beamform result as conventional phase-rotation-based beamform.

Since the complex signal generated by the proposed method is band limited as the result of filtering (Fig. 8c), down-sampling can be performed on the complex signal without causing aliasing. Fig. 9 compares the spectrum of the complex signal after decimation with that of the conventional method, where the sampling rate is reduced to $2f_c$. Actually, as indicated in Eq. (9), the spectrum of the complex signal can be derived by shifting the spectrum of the base-band signal in frequency by f_c.

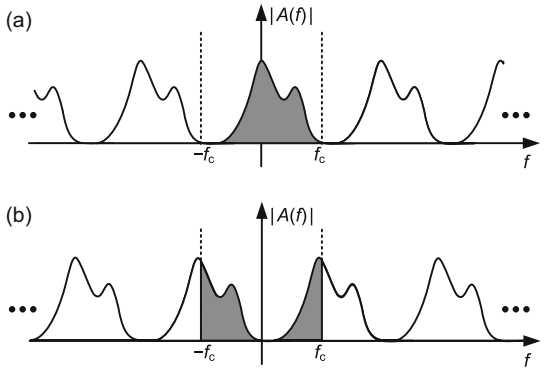

Fig. 9 Spectrum of the down-sampled base-band signal (a) and the down-sampled complex signal (b). The sampling frequency used here is $2f_c$, and the dark regions represent the base-band

The efficiency of the proposed method will be reduced when the number of taps of the low-pass filter is large. However, as indicated in the simulation (Figs. 4 and 6), the low-pass filter with a tap number of eight would provide sufficient demodulation accuracy for ultrasound imaging. The accuracy can be further improved by increasing the number of taps of the filter to 16, when the proposed method can reduce the number of multiplication operations by a factor of 1.5, compared with the conventional method.

Although the proposed method is implemented in a program on a PC-based ultrasound system, the proposed method is more suitable for hand-held ultrasound imaging devices, in which the computational resources are very limited.

5 Conclusions

The medical ultrasound imaging system requires efficient signal processing for generating multi-mode images or reducing hardware complexity. In this paper, an efficient quadrature demodulation method was proposed for ultrasound B-mode and color flow imaging to reduce the computational complexity. The performance of the proposed method was evaluated, and the results showed that the proposed method can provide a similar accuracy to that of the conventional quadrature demodulation, while reducing the operating time.

References

Agarwal, A., Yoo, Y.M., Schneider, F.K., *et al.*, 2007. New demodulation method for efficient phase-rotation-based beamforming. *IEEE Trans. Ultrason. Ferroelect. Freq. Contr.*, **54**(8):1656-1668. [doi:10.1109/TUFFC.2007.437]

Chang, J., Yen, J.T., Shung, K.K., 2007. A novel envelope detector for high-frame rate, high-frequency ultrasound imaging. *IEEE Trans. Ultrason. Ferroelect. Freq. Contr.*, **54**(9):1792-1801. [doi:10.1109/TUFFC.2007.463]

Fritsch, C., Ibanez, A., Parrilla, M., 1999. A digital envelope detection filter for real-time operation. *IEEE Trans. Instrum. Meas.*, **48**(6):1287-1293. [doi:10.1109/19.816150]

Gerneth, F., 2010. FIR Filter Algorithm Implementation Using Intel SSE Instructions—Optimizaing for Intel Atom Architecture. White Paper, 323411. Intel Corporation, CA, USA.

Hassan, M.A., Youssef, A.B.M., Kadah, Y.M., 2011. Embedded digital signal processing for digital ultrasound imaging. Proc. 28th National Radio Science Conf., p.1-10. [doi:10.1109/NRSC.2011.5873642]

Jensen, J.A., Svendsen, N.B., 1992. Calculation of pressure fields from arbitrarily shaped, apodized, and excited ultrasound transducers. *IEEE Trans. Ultrason. Ferroelect. Freq. Contr.*, **39**(2):262-267. [doi:10.1109/58.139123]

Jin, C., Chen, S.P., Qin, Z.D., *et al.*, 2010. A new scheme of coded ultrasound using Golay codes. *J. Zhejiang*

Univ.-Sci. C (Comput. & Electron.), **11**(6):476-480. [doi:10.1631/jzus.C0910353]

Lee, D.Y., Yoo, Y., Song, T.K., *et al.*, 2012. Adaptive dynamic quadrature demodulation with autoregressive spectral estimation in ultrasound imaging. *Biomed. Signal Process. Contr.*, **7**(4):371-378. [doi:10.1016/j.bspc.2011.06.010]

Levesque, P., Sawan, M., 2009. Real-time hand-held ultrasound medical-imaging device based on a new digital quadrature demodulation processor. *IEEE Trans. Ultrason. Ferroelect. Freq. Contr.*, **56**(8):1654-1665. [doi:10.1109/TUFFC.2009.1230]

Loupas, T., Powers, J.T., Gill, R.W., 1995. An axial velocity estimator for ultrasound blood flow imaging, based on a full evaluation of the Doppler equation by means of a two-dimensional autocorrelation approach. *IEEE Trans. Ultrason. Ferroelect. Freq. Contr.*, **42**(4):672-688. [doi:10.1109/58.393110]

Marple, S.L., 1999. Computing the discrete-time "analytic" signal via FFT. *IEEE Trans. Signal Process.*, **47**(9):2600-2603. [doi:10.1109/78.782222]

Pailoor, R., Pradhan, D., 2008. Digital Signal Processor (DSP) for Portable Ultrasound. Application Report, SPRAB18A. Texas Instruments, TX, USA.

Palmeri, M.L., McAleavey, S.A., Trahey, G.E., *et al.*, 2006. Ultrasonic tracking of acoustic radiation force-induced displacements in homogeneous media. *IEEE Trans. Ultrason. Ferroelect. Freq. Contr.*, **53**(7):1300-1313. [doi:10.1109/TUFFC.2006.1665078]

Reilly, A., Frazer, G., Boashash, B., 1994. Analytic signal generation—tips and traps. *IEEE Trans. Signal Process.*, **42**(11):3241-3245. [doi:10.1109/78.330385]

Thomas, L.J., 2005. Ultrasound imaging systems. *In*: Oppelt, A. (Ed.), Imaging Systems for Medical Diagnostics—Fundamentals, Technical Solutions and Applications for System Applying Ionizing Radiation, Nuclear Magnetic Resonance and Ultrasound. Publicis Corporate Publishing, Erlangen, p.732-820.

Zahiri-Azar, R., Salcudean, S.E., 2006. Motion estimation in ultrasound images using time domain cross correlation with prior estimates. *IEEE Trans. Biomed. Eng.*, **53**(10):1990-2000. [doi:10.1109/TBME.2006.881780]

Zahiri-Azar, R., Baghani, A., Salcudean, S.E., *et al.*, 2010. 2-D high-frame-rate dynamic elastography using delay compensated and angularly compounded motion vectors: preliminary results. *IEEE Trans. Ultrason. Ferroelect. Freq. Contr.*, **57**(11):2421-2436. [doi:10.1109/TUFFC.2010.1709]

Zahiri-Azar, R., Dickie, K., Pelissier, L., 2012. Real-time 1-D/2-D transient elastography on a standard ultrasound scanner using mechanically induced vibration. *IEEE Trans. Ultrason. Ferroelect. Freq. Contr.*, **59**(10):2167-2177. [doi:10.1109/TUFFC.2012.2443]

Zhao, H., Mo, L.Y.L., Gao, S.K., 2007. Barker-coded ultrasound color flow imaging: theoretical and practical design considerations. *IEEE Trans. Ultrason. Ferroelect. Freq. Contr.*, **54**(2):319-331. [doi:10.1109/TUFFC.2007.246]

Appendix: Derivation of the base-band signal in Eq. (3)

Substituting Eq. (1) into the first equation of Eq. (2) yields

$$I(n)=\sum_{i=0}^{M}h(i)\left[a(n-i)\cos(\omega_{\mathrm{c}}(n-i)+\varphi(n-i))\cdot\cos(\omega_{\mathrm{c}}(n-i)+\varphi_{\mathrm{c}})\right]. \tag{A1}$$

Using the trigonometric equation

$$\cos\alpha\cos\beta=\frac{\cos(\alpha-\beta)+\cos(\alpha+\beta)}{2}, \tag{A2}$$

Eq. (A1) can be rewritten as

$$I(n)=\sum_{i=0}^{M}h(i)\frac{a(n-i)}{2}\big[\cos(\varphi(n-i)-\varphi_{\mathrm{c}})+\cos(2\omega_{\mathrm{c}}(n-i)+\varphi(n-i)+\varphi_{\mathrm{c}})\big]. \tag{A3}$$

Consider the frequency characteristic of the low-pass filter $h(i)$, the component with higher frequency ($2\omega_{\mathrm{c}}$) in Eq. (A3) will be removed. Thus, Eq. (A3) can be simplified as

$$I(n)=\sum_{i=0}^{M}h(i)\frac{a(n-i)}{2}\cos(\varphi(n-i)-\varphi_{\mathrm{c}}). \tag{A4}$$

The resulting base-band signal in Eq. (A4) matches the passband of the low-pass filter. Due to the linear phase response of the FIR filter, the result of Eq. (A4) will approximately be a delayed replica of the base-band signal:

$$I(n)\approx\frac{a(n-d)}{2}\cos(\varphi(n-d)-\varphi_{\mathrm{c}}). \tag{A5}$$

Similarly, using the trigonometric equation

$$\cos\alpha\sin\beta=-\frac{\sin(\alpha-\beta)-\sin(\alpha+\beta)}{2}, \tag{A6}$$

the quadrature component of quadrature demodulation can be written as

$$Q(n)\approx-\frac{a(n-d)}{2}\sin(\varphi(n-d)-\varphi_{\mathrm{c}}). \tag{A7}$$

Eq. (3) can be derived by combining Eqs. (A5) and (A7), i.e.,

$$\begin{aligned}e(n)&=I(n)+\mathrm{j}Q(n)\\&=\frac{a(n-d)}{2}\cos(\varphi(n-d)-\varphi_{\mathrm{c}})\\&\quad-\mathrm{j}\frac{a(n-d)}{2}\sin(\varphi(n-d)-\varphi_{\mathrm{c}})\\&=\frac{a(n-d)}{2}\exp[-\mathrm{j}(\varphi(n-d)-\varphi_{\mathrm{c}})].\end{aligned} \tag{A8}$$